Atmospheric Research 101 (2011) 46–53

Contents lists available at ScienceDirect

Atmospheric Research

journal homepage: www.elsevier.com/locate/atmos

Characterization of the aerosol type using simultaneous measurements of the lidar ratio and estimations of the single scattering albedo

Vassilis Amiridis [a,*], Dimitrios Balis [b], Eleni Giannakaki [b], Stylianos Kazadzis [c], Antti Arola [d], Evangelos Gerasopoulos [c]

[a] Institute for Space Applications and Remote Sensing, National Observatory of Athens, Athens, Greece
[b] Laboratory of Atmospheric Physics, Aristotle University of Thessaloniki, Thessaloniki, Greece
[c] Institute of Environmental Research and Sustainable Development, National Observatory of Athens, Athens, Greece
[d] Finnish Meteorological Institute, Kuopio Unit, Kuopio, Finland

ARTICLE INFO

Article history:
Received 4 October 2010
Received in revised form 15 December 2010
Accepted 10 January 2011

Keywords:
Aerosol lidar
Single scattering albedo

ABSTRACT

Lidar measurements of the vertical distribution of the aerosol extinction and backscatter coefficient and the corresponding extinction to backscatter ratio (so-called lidar ratio) at 355 nm have been performed at Thessaloniki, Greece using a Raman lidar system in the frame of the EARLINET for the period 2001–2005. Coincident spectral UV irradiance measurements, total ozone observations and aerosol optical depth estimates were available from a double Brewer spectroradiometer. The retrieval of single scattering albedo employed the Brewer global irradiance measurements and radiative transfer modeling. Vertically averaged values of the lidar ratio ranged from a minimum of 16 sr to a maximum value of 90 sr, while the effective single scattering albedo ranged from 0.78 to 1.00. The mean value of the lidar ratio for the dataset under study was 45.5 ± 21.0 sr while the average value of the single scattering albedo was 0.94 ± 0.05. For the majority of our measurements (80%) the single scattering albedo found to be greater than 0.90. Using additional information from backward trajectory calculations and lidar-derived free tropospheric contribution of aerosols in the columnar aerosol optical depth, it is shown that the combined use of the directly measured lidar ratio, and the indirectly estimated single scattering albedo, leads to a better characterization of the aerosol type probed.

1. Introduction

Tropospheric aerosols play an important role in Earth's radiation budget through the scattering and absorption of Sun and Earth radiation (IPCC, 2007). In order to address aerosol radiative forcing, a proper aerosol type characterization is required. This task could be very difficult in regions with strong mixing of air masses from different aerosol sources. Within the eastern Mediterranean, the Aegean Sea and the coastal part of continental Greece are in a geographical position where in addition to local sources, aerosols from different sources converge (Lelieveld et al., 2002). In addition to the maritime aerosols from sea spray and mineral dust from North Africa, anthropogenic aerosols from the highly populated urban centers and industrial areas of central and eastern Europe, as well as seasonal biomass burning are present (Balis et al., 2003, 2004; Amiridis et al., 2005, 2009; Kazadzis et al., 2007). In geographical areas like Greece, considered as "crossroads" of air pollution from different sources, the aerosol type can only be characterized by a combination of information coming from various remote sensing and in-situ measurements. Synergistic use of optical information is required to proper identify the aerosol content and characteristics. In this context, lidar measurements of particle optical properties with high spatial and temporal resolution are extremely useful since they give detailed

* Corresponding author. National Observatory of Athens, Institute for Space Applications & Remote Sensing, Metaxa and Vas. Paulou str. GR-15236 Penteli, Greece. Tel.: +30 2108109116; fax: +30 2106138343.
E-mail address: vamoir@noa.gr (V. Amiridis).
URL: http://www.space.noa.gr/ (V. Amiridis).

0169-8095/$ – see front matter © 2011 Elsevier B.V. All rights reserved.
doi:10.1016/j.atmosres.2011.01.010

information on the occurrence, extent, and development of aerosol structures.

The combination of lidar measurements with estimates of the aerosol absorption could potentially help to characterize the aerosol burden over an area. For the determination of the absorption of solar radiation by aerosols in the atmosphere, one can infer the single scattering albedo (SSA) utilizing the Mie-scattering code and a radiative transfer model in conjunction with remote sensing measurements (transmission and size distribution measurements). Following this approach, we infer the effective columnar SSA from Brewer spectroradiometer global irradiance measurements with the aid of radiative transfer modeling (Bais et al., 2005). Then, we investigate the potential of the combined use of the directly measured extinction to backscatter ratio, the so-called lidar ratio (LR), and the indirectly estimated SSA in conjunction with backward trajectory calculations for the better characterization of the aerosol type. The lidar ratio is a quantity that is directly measured by a Raman lidar (Ansmann et al., 1992; Noh et al., 2007) and the SSA is one of the most dominant input factors that determine the aerosol type in radiative transfer models (e.g. Sanchez et al., 1994; Liou and Takano, 1994; Kylling et al., 1998; Li et al., 2004). Both depend on the microphysical properties of the aerosols and therefore their value can be used for the characterization of the aerosol type.

2. Data and methodology

2.1. Lidar data

At the Laboratory of Atmospheric Physics of the Aristotle University of Thessaloniki (LAP-AUTH/40.5° N, 22.9° E), a two wavelength combined Raman elastic-backscatter lidar has been used since 2001 (Balis et al., 2004; Amiridis et al., 2005) to perform continuous measurements of suspended aerosol particles in the Planetary Boundary Layer (PBL) and the lower Free Troposphere (FT). The LAP-AUTH lidar is based on the second and third harmonic frequency of a pulsed Nd:YAG laser, which emits pulses of 300 and 120 mJ output energy at 532 and 355 nm, respectively, with a 10 Hz repetition rate. The optical receiver is a 500 mm diameter Newtonian telescope with 0.7–3 mrad adjustable field-of-view. Three Hamamatsu R7400P-06 photomultipliers are used to detect the lidar signals at 532, 355 and 387 nm with 15 m height resolution. More details about the technical characteristics and the measurement principles can be found in the foregoing two references. The lidar system of LAP and the algorithms implemented is part of the European Aerosol Research Lidar Network (EARLINET) and were successfully intercompared (Matthias et al., 2004; Böckmann et al., 2004; Pappalardo et al., 2004).

2.2. Brewer spectroradiometer measurements

The Brewer spectroradiometer of the LAP-AUTH is a double monochromator consisting of two identical spectrometers equipped with holographic diffraction gratings (3600 lines/mm) operating in the first order. The operational spectral range of the instrument for the global irradiance measurements is 287.5–366.0 nm, and its spectral resolution is 0.55 at full width at half maximum (FWHM). Details on the operation and calibration procedures are given in Garane et al. (2005). The spectral aerosol optical depth (AOD) is determined by comparing the measured cloud-free spectral direct irradiance at the surface to the direct irradiance which is calculated from the transfer of the high resolution extraterrestrial spectrum ATLAS 3 (Van Hoosier, 1996) through the atmosphere using the Beer's law and accounting only for molecular absorption (mainly O3 and SO2) and Rayleigh scattering. The method that was used to calibrate the direct irradiance spectra and retrieve the AOD is described in Kazadzis et al. (2005).

2.3. Radiative transfer modeling and SSA retrieval

Look-up tables (LUT) describing the modification of clear-sky global irradiances by the aerosol single scattering albedo, as a function of aerosol optical depth, and solar zenith angle (SZA) were composed using radiative transfer model calculations of LibRadtran 0.99 package and UVSPEC DISORT version (Mayer and Kylling, 2005). The model-derived relations are combined with UV irradiances at 355 nm at the surface and the AOD measured with a Brewer MkIII spectroradiometer, with the aim to calculate an effective SSA at 355 nm. The methodology and uncertainties of this method are quantitatively discussed in Bais et al. (2005).

2.4. Backward trajectories

Four-day back trajectories were computed for the days of interest, using the Hybrid Single-Particle Lagrangian Integrated Trajectory (HYSPLIT) model (Draxler and Rolph, 2003), which uses the meteorological data produced by the National Weather Service ETA Model to compute advection and dispersion of air-parcels. We used HYSPLIT to generate 4-day back trajectories for air-parcels arriving over our site in Thessaloniki for all the 38 days of available simultaneous Raman lidar and Brewer measurements. The atmospheric trajectories were calculated for the arrival time of 19:00 UTC, which corresponds approximately to the time of the routine Raman lidar observations at sunset.

3. Results and discussion

Lidar measurements of the vertical distribution of the aerosol and backscatter coefficient and the corresponding LR have been performed at Thessaloniki, Greece, using a Raman lidar system in the frame of the EARLINET for the period 2001–2005. Coincident spectral UV irradiance measurements, total ozone observations and AOD estimates were available from a double Brewer spectroradiometer whenever lidar measurements were obtained. To combine the measured LR with the retrieved SSA from global irradiance measurements and radiative transfer modeling for the characterization of the aerosol load, first we have to assume that nighttime lidar data and daytime sunphotometric data are referring to the same aerosol burden. To do that, we only keep a combination of data in which the AOD diurnal variability is not significant. Specifically, only the days with AOD difference between daytime/nighttime measurements less than 0.05 were kept in our dataset. For each day, we compare daytime Brewer AOD measurements at 355 nm with nighttime Raman-lidar AOD at 355 nm. Columnar AOD is difficult to be calculated with

Raman lidar due to the incomplete overlap between the laser beam and the receiver field of view which significantly affects lidar observations of particle optical properties in the near-field range. Thessaloniki's lidar transmitted laser beam overlaps completely with the receiver's field of view, usually at heights around 1500 m for 355 nm and 1000 m for 532 nm, because of the different geometries with which the two wavelengths are emitted to the atmosphere (Amiridis et al., 2005). At 355 nm, we apply an overlap correction on the basis of a simple technique proposed by Wandinger and Ansmann (2002), down to the height where the overlap function is equal to 0.7. This correction allows extending the profile in most cases down to 700–1000 m above sea level. An application of this methodology and its experimental verification is presented by Balis et al. (2002). Then, the AOD at 355 nm is calculated by integrating the Raman-retrieved nighttime aerosol extinction profile assuming that the lowest extinction value is representative down to the surface. This is a very reasonable assumption, since the PBL is still fully developed at sunset and is a common approach in lidar studies (e.g., Amiridis et al., 2005; Mattis et al., 2004; Matthias et al., 2004). Following this methodology, 38 dates with AOD differences less than 0.05 were found. For the same days, the backscatter-related Angström exponent (BRAE), retrieved from backscatter coefficient profiles at 355 and 532 nm showed a diurnal variability less than 0.2, indicating that the daytime/nighttime measurements refer to almost the same aerosol burden over Thessaloniki.

For the 38 days of our measurements when the aforementioned restrictions were valid, the estimated effective SSA at 355 nm and the vertically averaged LR at 355 nm is presented in Fig. 1. The error bars for the LR stand for the standard deviation of the vertical averaging, while the error bars for the SSA represent the standard deviation arise from averaging SSAs over a time frame identical with the time averaging window used on lidar signals to perform Raman calculations. The columnar LR values presented refer to the weighted vertical averaged values, where for weight we consider the statistical error emerging from the lidar ratio calculation. This averaging method is applied to minimize the effect of lidar ratios with great retrieval uncertainties on the averaging. Such values usually appear in the range of the free-tropospheric aerosol free region used in the lidar inversions. Regions of incomplete overlap are excluded from the averaging. Vertically averaged values of the LR ranged from a minimum of 16 sr to a maximum of 90 sr, while SSA values ranged from 0.78 to 1.00. The mean value of the LR for the dataset under study was 45.5 ± 21.0 sr while the average value of SSA was 0.94 ± 0.05. For the majority of our measurements (80%) the SSA found to be greater than 0.90. From Fig. 1 it is evident that strong absorption with SSA values less than 0.85 is in all cases accompanied with small LRs of the order of 20 sr.

In order to explain the observed variability in the LR and SSA values, we tried to exclude from Fig. 1 Saharan dust and smoke special cases of aerosol presence over Thessaloniki. For the 38 days of the dataset under study, the aerosol burden over Thessaloniki was influenced by Saharan dust particles for 11 days, while 8 days were identified when smoke was advected from biomass burning activities in adjacent regions. In Fig. 2, the relations between the LR and SSA for Saharan dust (upper panel) and smoke from biomass burning (lower panel) are presented. For the Saharan dust cases (see Fig. 2, upper panel) the mean LR was found to be 41.4 ± 17.3 sr, and the mean SSA, 0.95 ± 0.03. LR values ranged from 18.3 to 80.9 sr and SSA values ranged from 0.91 to 1.00. LR values reported here for dust is presented and discussed in detail in Balis et al. (2004). SSA values of dust are additionally affected by boundary layer aerosols of local origin. Following the literature, SSA values for dust particles should be lower, since it is believed that these particles are strongly absorbing (e.g. Patterson and McMahon, 1984). However, absorption retrievals from ground-based remote sensing sky radiance measurements (Cattrall et al., 2003), showed that the observed absorption of wind-blown African dust is much less than that assumed by mineral dust models, which are constructed from laboratory measurements of Saharan aerosols on filter pads (Patterson and McMahon, 1984). The retrieved SSAs in this study agree well with values obtained by different remote sensing methods and suggest that a weakly absorbing model of African dust is more appropriate for climate studies (Miller

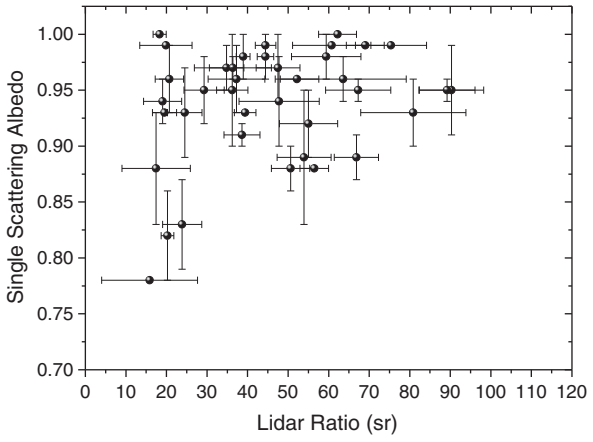

Fig. 1. Effective single scattering albedo at 355 nm versus mean columnar lidar ratio at 355 nm for 38 days of coincident sunphotometric and Raman lidar measurements in the period 2001–2005.

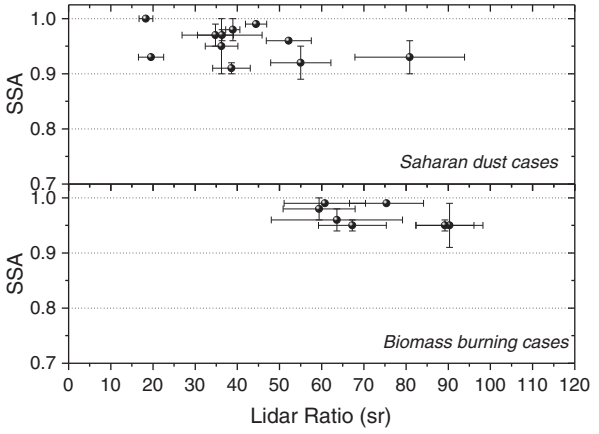

Fig. 2. Effective single scattering albedo at 355 nm versus mean columnar lidar ratio at 355 nm for Saharan dust cases (upper panel) and for smoke cases (lower panel) for the period 2001–2005.

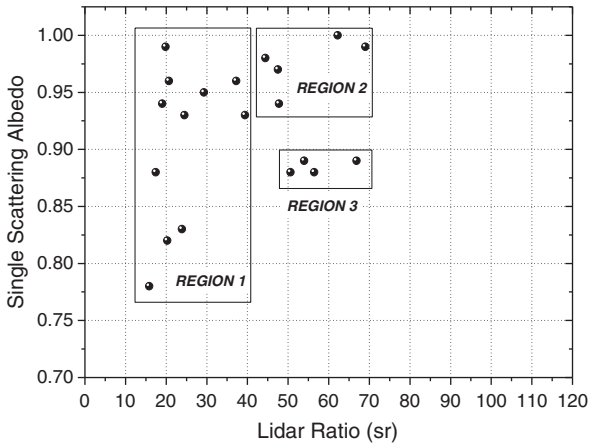

Fig. 3. Effective single scattering albedo at 355 nm versus mean columnar lidar ratio at 355 nm for 20 days of coincident sunphotometric and Raman lidar measurements for the period 2001–2005, excluding Saharan dust and smoke cases.

and Tegen, 1998; Myhre and Stordal, 2001; Perlwitz et al., 2001). We have to mention that for SSA retrievals presented here, we did not consider the non-spherical shape of the dust particles. Our SSA retrieval is based on measurements of both AOD and global UV irradiance. As discussed by Dubovik et al. (2000), the proportion between total extinction and scattering is not very sensitive to the shape. For instance, Kahnert et al. (2007), used in their study the same SSA retrieval regardless of the shape.

In Fig. 2 (lower panel), LR and SSA values are presented for the eight days of smoke presence over Thessaloniki. Smoke from biomass burning activities across Russia in the latitudinal belt between 45°N and 55°N, as well as in Eastern Europe (Baltic countries, Western Russia, Belarus, and the Ukraine) (Amiridis et al., 2010), are often observed over Thessaloniki (Amiridis et al., 2009). Smoke presence is identified by the use of back trajectories, particle dispersion modeling and satellite hot spot fire detection (see Amiridis et al., 2009 for details). Forest fires in Russia are a major source of pollution in the Northern Hemisphere (Wotawa et al., 2001). For that reason, there has been increased interest in recent years to assess the impact of these fires on climate (e.g. Kasischke and Bruhwiler, 2003). Following Fig. 2 (lower panel), the mean LR for smoke from Russian agricultural fires was found to be 72.3 ± 13.0 sr, and the mean SSA, 0.97 ± 0.02. LR values ranged from 59.4 to 90.3 sr and SSA values ranged from 0.95 to 0.99. The variability of the LR for smoke particles can be attributed to the fact that the fire regions are located in variable distances from Thessaloniki which affects the optical characteristics and microphysical properties (such as the effective radius) of the observed smoke aerosols due to different ageing processes, depending also to the meteorological conditions responsible for the speed of the smoke plume. The LR values reported here are not representative for smoke particles, also because the vertical averaging has been applied to the complete lidar profile and not in the height ranges of smoke presence. Thus, the LR values are representative of the entire atmospheric column, including local aerosol emissions. However, LR values for smoke particles for the days presented here can be found in Amiridis et al. (2009). Considering SSA, the values reported in Fig. 2 (lower panel) are again not representative for smoke particles. These values are referring again to the atmospheric column and they are contaminated with urban aerosols that are emitted in the atmosphere from the city's activities. However, SSA values presented here were expected to reach smaller values, since the absorption properties of smoke should be reflected in a certain level to our retrievals. However, it is evident from the literature that particle growth by coagulation and condensation increases the amount of light scattered in the evolving smoke plume and decreases the mass absorption efficiency and, consequently, increases the SSA (Abel et al., 2003; Reid et al., 2005). Evidence suggests that most particle growth in size and mass occurs on fairly short time scales (Abel et al., 2003; Reid et al., 1998). Calculations (e.g., Turco and Yu, 1997) indicate that after a plume has dispersed into a regional haze or is undergoing long-range transport, particle coagulation is the significant mechanism for particle growth over long enough timescales. If this evolution of smoke particles is not properly accounted for, large errors may result in calculations of their RF on regional and global scales (Müller et al., 2005).

Excluding the severe Saharan dust and smoke episodes presented in Fig. 2, the relation between the mean columnar LR and the estimated effective SSA for the 20 remaining cases is presented in Fig. 3. To investigate the variability of the optical parameters in this figure, we first calculated the free tropospheric contribution to the total aerosol load. With this method we tried to separate cases where local (small free tropospheric contribution) or transported (great free tropospheric contribution) pollution is mostly responsible for the observed columnar results. This approach has been followed since it is well known that even excluding dust and smoke cases, the free tropospheric air quality over the Mediterranean is reduced by European pollution particularly during summer, whereas in the free troposphere pollution is largely determined by trans-boundary transport (Zerefos et al., 2000; Lelieveld et al., 2002; Amiridis et al., 2005; Gerasopoulos et al., 2006, 2007; Fotiadi et al., 2006; Kazadzis et al., 2007). Amiridis et al. (2005) showed that free tropospheric particles over Thessaloniki contributed from 5% (clean free troposphere conditions) to 55% to the total aerosol optical depth, while the average contribution was about 30%. To estimate the contribution of light extinction by free tropospheric particles to the total tropospheric optical depth, we calculated the AOD in the PBL and the FT separately. In order to integrate the extinction coefficient derived by the Raman lidar in these two height intervals, first we have determined the PBL height. In lidar research, one can use as the PBL height that height, below which most of the aerosol is confined, even if this layer is not in every case a well mixed layer (Matthias and Bösenberg, 2002; Bösenberg et al., 2003; Mok and Rudowicz, 2004; De Tomasi and Perrone, 2006). To estimate the PBL height in our data, the derivative of the range-corrected lidar signal is calculated for each profile. The first derivative minimum which results from the strong decrease in aerosol backscatter due to lower particle concentration and humidity above this height is considered as the PBL height. The method is simple and it has been used since many years (e.g. Flamant et al., 1997; Menut et al., 1999). Using PBL height estimations, we found that when the free tropospheric contribution in the total aerosol load was below 35%, the LR also showed small values, below 40 sr. For the same cases we also examined the

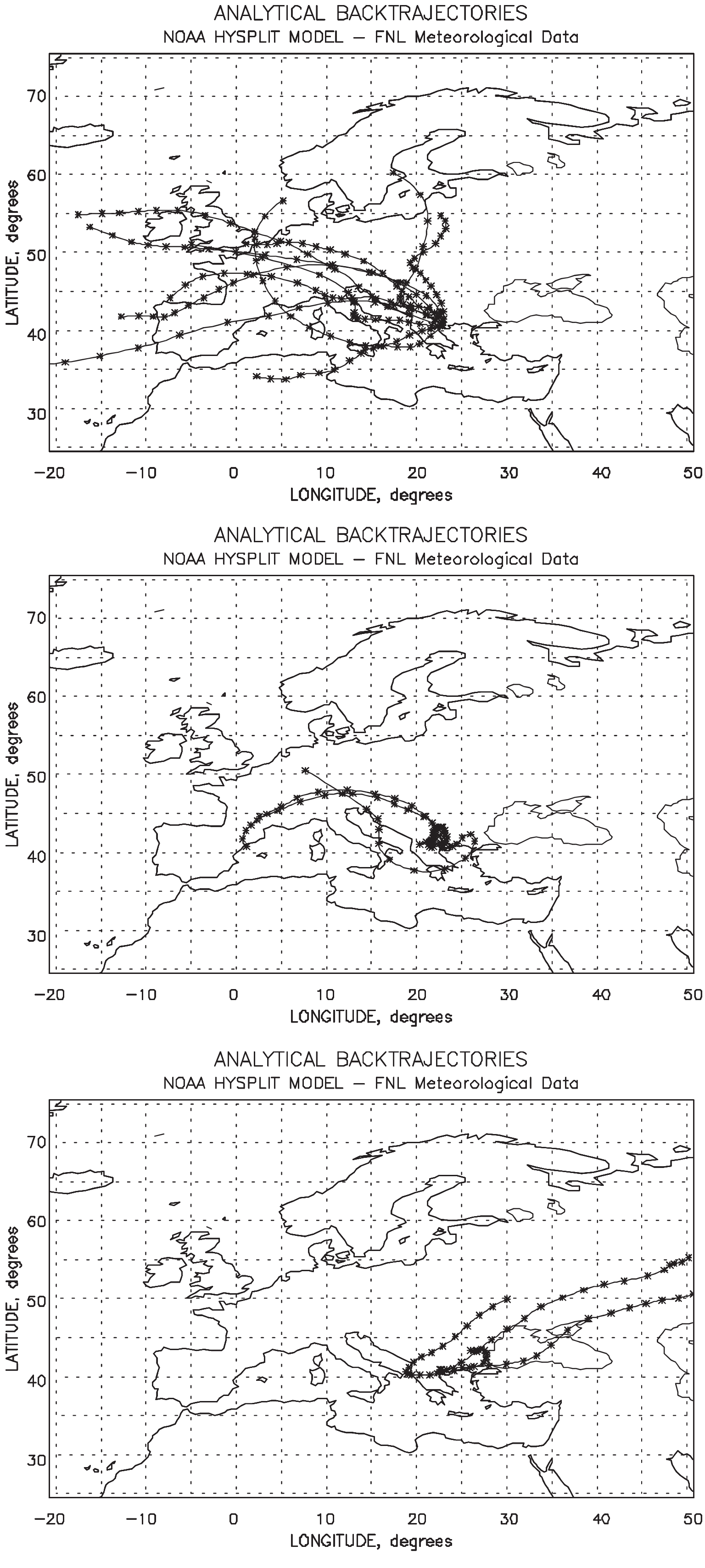
ANALYTICAL BACKTRAJECTORIES
NOAA HYSPLIT MODEL — FNL Meteorological Data
LATITUDE, degrees
30
40
50
60
70
−20
−10
0
10
20
30
40
50
LONGITUDE, degrees
ANALYTICAL BACKTRAJECTORIES
NOAA HYSPLIT MODEL — FNL Meteorological Data
LATITUDE, degrees
30
40
50
60
70
−20
−10
0
10
20
30
40
50
LONGITUDE, degrees
ANALYTICAL BACKTRAJECTORIES
NOAA HYSPLIT MODEL — FNL Meteorological Data
LATITUDE, degrees
30
40
50
60
70
−20
−10
0
10
20
30
40
50
LONGITUDE, degrees

4-day back trajectories for the air-parcels arriving over Thessaloniki site at the altitude of 1500 m which according to the mean backscatter profile for Thessaloniki (see Amiridis et al., 2005), represents the height with the maximum aerosol loading. The atmospheric trajectories were calculated for the arrival time of 19:00 UTC, which correspond approximately to the time of the routine Raman lidar observations at sunset in the frame of EARLINET. These trajectories (see Fig. 4(a)), indicate prevailing Western and North-Western flows for the region of Fig. 3 where LR values are below 40 sr, indicating the possible advection of continental aerosol from Europe. In the following we refer to this region of Fig. 3 as Region 1. Taking into account that small values of LR indicate maritime component (of the order of 25 sr according to Müller et al., 2007), it is likely that Thessaloniki's maritime background influences LRs in this region of small free-tropospheric contribution. The effective SSA of region 1 showed a great variability with values ranged from 0.78 to 0.99. Low SSA values are rather unexpected for this region of small LRs, indicative of strong maritime component. However, Thessaloniki's urban component and the continental free-tropospheric contribution (ranging between 10% and 35%) are considered to alter aerosol absorption, as it is evident for the cases of small SSAs.

For LR values greater than 40 sr, we observe in Fig. 3 that the effective SSA shows less variability, with values ranging from 0.87 to 1.00. Lidar-calculated free tropospheric contribution for these cases is always greater than 42% reaching even 59%. 4-day back trajectories at 1500 m for these days (see Fig. 4(b) and (c)) indicate that the higher values of LR, already associated with polluted events with great free tropospheric contribution ($50 \pm 7\%$) are connected with transport of air masses from West and North-West directions. For these cases, the differences observed in our optical parameters in relation with days corresponding in Region 1 is the enhancement of the free tropospheric contribution. In conclusion, for Western and Northwestern flows, the LR becomes greater than 40 sr and has an average value of 54 ± 11 sr, only when the free tropospheric contribution becomes significant. The average effective SSA for these days is 0.98 ± 0.02, indicating enhanced scattering properties and small variation. We observed this behavior for 5 days in our dataset and we are referring in this region of Fig. 3 as Region 2.

For the remaining four days of our measurements (Region 3 of Fig. 3) where the SSA is almost constant, also indicating more absorbing particles (0.88 ± 0.01), the back trajectories 'see Fig. 4(c)' showed that the air masses were advected over Thessaloniki from the North and North-eastern directions. The free tropospheric contribution for these cases was found $50 \pm 8\%$ and the average LR, 57 ± 7 sr. These days exhibit well defined optical properties, namely almost constant LR and SSA values, a significant free tropospheric contribution and a well defined pattern as it matters the origin of air-masses, indicating always Northeastern flows. These properties are attributed to the transportation of air masses over Thessaloniki from industrial areas (e.g. Maritsa, Bulgarian electricity power plants, see Koukouli et al., 2010) with enhanced absorbing properties.

4. Conclusions

It has been demonstrated that the combined use of the estimated SSA and the measured LR leads to a better characterization of the aerosol type probed, in the case of homogeneous aerosol layers. Our findings showed enhanced aerosol absorption for transport of air masses from North-eastern directions to Thessaloniki. The enhanced absorption was attributed to aerosol particles transported from Bulgarian electricity power plants and the observed cases were always accompanied with significant free tropospheric contribution. For the Western and North-western flows, the LR was found to be less than 40 sr, indicative of a strong maritime component, with variable SSAs, ranging from 0.78 to 0.99. The effective SSA estimated was found to be weighted by the local sources and the boundary layer (mainly soot) in cases where the free tropospheric contribution is rather low. These particles were found to alter the total columnar absorption in the absence of free tropospheric particles with enhanced scattering properties. LR became greater than 40 sr only when the free tropospheric contribution was significant. The average effective SSA for these days was found to be 0.98 ± 0.02, indicating enhanced scattering properties and small variation.

It is crucial to perform such measurements in parallel in order to achieve a significant amount of coincident data of SSA and LR, which will help to refine and validate the proposed approach. This information can be further used as input to radiative transfer models. In case of high aerosol load the estimated optical parameters at the Earth's surface may not be representative for the whole aerosol column.

Acknowledgments

This work was funded by the European Commission in the framework of EARLINET project (EVR1-CT1999-40003). Air mass back trajectories for Thessaloniki were produced with the Hybrid Single-Particle Lagrangian Integrated Trajectory model (NOAA). SK would like to acknowledge the Marie Curie project ACI-UV, PERG05-GA-2009-247492.

References

Abel, S.J., Haywood, J.M., Haywood, E.J., Li, J., Buseck, P.R., 2003. Evolution of biomass burning aerosol properties from an agricultural fire in southern Africa. Geophysical Research Letters 30 (15), 1783. doi:10.1029/2003GL017342.

Amiridis, V., Balis, D.S., Kazadzis, S., Bais, A., Giannakaki, E., Papayannis, A., Zerefos, C., 2005. Four-year aerosol observations with a Raman lidar at Thessaloniki, Greece, in the framework of European Aerosol Research Lidar Network (EARLINET). Journal of Geophysical Research 110, D21203. doi:10.1029/2005JD006190.

Amiridis, V., Balis, D.S., Giannakaki, E., Stohl, A., Kazadzis, S., Koukouli, M.E., Zanis, P., 2009. Optical characteristics of biomass burning aerosols over Southeastern Europe determined from UV-Raman lidar measurements. Atmospheric Chemistry and Physics 9, 2431–2440.

Amiridis, V., Giannakaki, E., Balis, D.S., Gerasopoulos, E., Pytharoulis, I., Zanis, P., Kazadzis, S., Melas, D., Zerefos, C., 2010. Smoke injection heights from agricultural burning in Eastern Europe as seen by CALIPSO. Atmospheric Chemistry and Physics 10, 11567–11576. doi:10.5194/acp-10-11567-2010.

Ansmann, A., Wandinger, U., Riebesell, M., Weitkamp, C., Michaelis, W., 1992. Independent measurement of extinction and backscatter profiles in

Fig. 4. Analytical 4-day backward trajectories for the arrival height of 1500 m over Thessaloniki, at 19:00 UTC, corresponding to Regions 1, 2 and 3 of Fig. 3.

cirrus clouds using a combined Raman elastic-backscatter lidar. Applied Optics 31, 7113.
Bais, A.F., Kazantzidis, A., Kazadzis, S., Balis, D.S., Zerefos, C.S., Meleti, C., 2005. Deriving an effective aerosol single scattering albedo from spectral surface UV irradiance measurements. Atmospheric Environment 39 (6), 1093–1102.
Balis, D., Amiridis, V., Zerefos, C., Papayannis, A., 2002. Verification of the experimental determination of the lidar overlap profile by a Raman lidar, paper presented at International Laser Radar Conference. Def. Res. and Dev. Can, Quebec, B. C., Canada.
Balis, D.S., Amiridis, V., Zerefos, C., Gerasopoulos, E., Andreae, M., Zanis, P., Kazantzidis, A., Kazadzis, S., Papayannis, A., 2003. Raman lidar and sunphotometric measurements of aerosol optical properties over Thessaloniki, Greece during a biomass burning episode. Atmospheric Environment 37, 4529–4538.
Balis, D., Amiridis, V., Nickovic, S., Papayannis, A., Zerefos, C., 2004. Optical properties of Saharan dust layers as detected by a Raman lidar at Thessaloniki, Greece. Geophysical Research Letters 31, L13104. doi:10.1029/2004GL019881.
Böckmann, C., Wandinger, U., Ansmann, A., Bösenberg, J., Amiridis, V., Boselli, A., Delaval, A., De Tomasi, F., Frioud, M., Grigovov, I.V., Hagard, A., Iarlori, M., Komguem, L., Kreipl, S., Larcheveque, G., Matthias, V., Papayan-nis, A., Pappalardo, G., Rocadenbosch, F., Rodrigues, J.A., Schneider, J., Scherbakov, V., Wieger, M., 2004. Aerosol lidar intercomparison in the framework of the EARLINET project: 2. Aerosol backscatter algorithms. Applied Optics 43, 977–989.
Bösenberg, J., Matthias, V., Amodeo, A., Amoiridis, V., Ansmann, A., Baldasano, J.M., Balin, I., Böckmann, C., Boselli, A., Carlsson, G., Chaykovski, A., Chourdakis, G., Comeron, A., DeTomasi, F., Eixmann, R., Freudenthaler, V., Giehl, H., Grigorov, I., Hågård, A., Iarlori, M., Kirsche, A., Kolarov, G., Komguem, L., Kreipl, S., Kumpf, W., Larchevêque, G., Linne, H., Matthey, R., Mattis, I., Mekler, A., Mironova, I., Mitev, V., Mona, L., Müller, D., Music, S., Nickovic, S., Pandolfi, M., Papayannis, A., Pappalardo, G., Pelon, J., Peres, C., Perrone, R.M., Persson, R., Resendes, D.P., Rizi, V., Rocadenbosch, F., Rodriguez, J., Sauvage, L., Schneidenbach, L., Schumacher, R., Shcherbakov, V., Simeonov, V., Sobolewski, P., Spinelli, N., Stachlewska, I., Stoyanov, D., Trickl, T., Tsaknakis, G., Vaughan, G., Wandinger, U., Wang, X., Wiegner, M., Zavrtanik, M., Zerefos, C., 2003. EARLINET: 'A European Aerosol Research Lidar Network to Establish an Aerosol Climatology', Report of the Max-Planck-Institute for Meteorology, p. 348.
Cattrall, C., Carder, K.L., Gordon, H.R., 2003. Columnar aerosol single-scattering albedo and phase function retrieved from sky radiance over the ocean: measurements of Saharan dust. Journal of Geophysical Research 108 (D9), 4287.
De Tomasi, F., Perrone, Maria Rita, 2006. PBL and dust layer seasonal evolution by lidar and radiosounding measurements over a peninsular site. Atmospheric Research 80, 86–103.
Draxler, R. R. and Rolph, G. D., 2003, HYSPLIT (HYbrid single-particle Lagrangian integrated trajectory) Model access via NOAA ARL READY Website (http://www.arl.noaa.gov/ready/hysplit4.html), NOAA Air Resources Lab., Silver Spring, MD, USA.
Dubovik, et al., 2000. Accuracy assessments of aerosol optical properties retrieved from Aerosol Robotic Network (AERONET) Sun and sky radiance measurements. Journal of Geophysical Research 105 (D8), 9791–9806.
Flamant, C., Pelon, J., Flamant, P., Durand, P., 1997. Lidar determination of the entrainment zone thickness at the top of the unstable marine atmospheric boundary layer. Boundary Layer Meteorology 83, 247–284.
Fotiadi, A., Hatzianastassiou, N., Drakakis, E., Matsoukas, C., Pavlakis, K.G., Hatzidimitriou, D., Gerasopoulos, E., Mihalopoulos, N., Vardavas, I., 2006. Aerosol physical and optical properties in the eastern Mediterranean Basin, Crete, from Aerosol Robotic Network Data. Atmospheric Chemistry and Physics 6, 5399–5413.
Garane, K., Bais, A.F., Tourpali, K., Meleti, C., Zerefos, C., Kazadzis, S., 2005. Variability of spectral UV irradiance at Thessaloniki, Greece, from 15 years measurement. Proceedings of SPIE - The International Society for Optical Engineering 5886, 1–10.
Gerasopoulos, E., Kouvarakis, G., Babasakalis, P., Vrekoussis, M., Putaud, J.P., Mihalopoulos, N., 2006. Origin and variability of particulate matter (PM10) mass concentrations over the eastern Mediterranean. Atmospheric Environment 40, 4679–4690. doi:10.1016/j.atmosenv.2006.04.020.
Gerasopoulos, E., Koulouri, E., Kalivitis, N., Kouvarakis, G., Saarikoski, S., Mäkelä, T., Hillamo, R., Mihalopoulos, N., 2007. Size-segregated mass distributions of aerosols over Eastern Mediterranean: seasonal variability and comparison with AERONET columnar size-distributions. Atmospheric Chemistry and Physics 7, 2551–2561.
Intergovernmental Panel on Climate Change (IPCC), 2007. Climate Change, 2007, The Physical Science Basis. In: Solomon, S., Qin, D., Manning, M., Chen, Z., Marquis, M., Averyt, K.B., Tignor, M., Miller, H.L. (Eds.), Contribution of Working Group I to the Fourth Assessment Report of the Intergovernmental Panel on Climate Change. Cambridge University Press, Cambridge. 996 pp.
Kahnert, M., Nousiainen, T., Räisänen, P., 2007. Mie simulations as an error source in mineral aerosol radiative forcing calculations. Quarterly Journal Royal Meteorological Society 133, 299–307. doi:10.1002/qj.40.
Kasischke, E.S., Bruhwiler, L.P., 2003. Emissions of carbon dioxide, carbon monoxide, and methane from boreal forest fires in 1998. Journal of Geophysical Research 108 (D1), 8146. doi:10.1029/2001JD000461.
Kazadzis, S., Bais, A., Kouremeti, N., Gerasopoulos, E., Garane, K., Blumthaler, M., Schallhart, B., Cede, A., 2005. Direct spectral measurements with a Brewer spectroradiometer: absolute calibration and aerosol optical depth retrieval. Applied Optics 44 (9), 1681–1690.
Kazadzis, S., Bais, A., Amiridis, V., Balis, D., Meleti, C., Kouremeti, N., Zerefos, C., Rapsomanikis, S., Petrakakis, M., Kelesis, A., Tzoumaka, P., Kelektsoglou, K., 2007. Nine years of UV aerosol optical depth measurements at Thessaloniki, Greece. Atmospheric Chemistry and Physics 7, 2091–2101.
Koukouli, M.E., Kazadzis, S., Amiridis, V., Ichoku, C., Balis, D., Bais, A., 2010. Signs of a negative trend in the MODIS Aerosol Optical Depth over the Southern Balkans, Atmospheric Environment 44, 1219–1228.
Kylling, A., Bais, A.F., Blumthaler, M., Shreder, J., Zerefos, C.S., 1998. UV irradiances during the PAUR campaign: comparison between measurement and model simulations. Journal of Geophysical Research 103 (D20), 26,051–26,060.
Lelieveld, J., Berresheim, H., Borrmann, S., Crutzen, P.J., Dentener, F.J., Fischer, H., Feichter, J., Flatau, P.J., Heland, J., Holzinger, R., Korrmann, R., Lawrence, M.G., Levin, Z., Markowicz, K.M., Mihalopoulos, N., Minikin, A., Ramanathan, V., De Reus, M., Roelofs, G.J., Scheeren, H.A., Sciare, J., Schlager, H., Schultz, M., Siegmund, P., Steil, B., Stephanou, E.G., Stier, P., Traub, M., Warneke, C., Williams, J., Ziereis, H., 2002. Global air pollution crossroads over the Mediterranean. Science 298, 794–799.
Li, Z., Goloub, P., Devaux, C., Gu, X., Qiao, Y., Zhao, F., Chen, H., 2004. Aerosol polarized phase function and single-scattering albedo retrieved from ground-based measurements. Atmospheric Research 71, 233–241.
Liou, K.N., Takano, Y., 1994. Light scattering by nonspherical particles: remote sensing and climatic implications. Atmospheric Research 31, 271–298.
Matthias, V., Bösenberg, J., 2002. Aerosol climatology for the planetary boundary layer derived from regular lidar measurements. Atmospheric Research 63, 221–245.
Matthias, V., Freudenthaler, V., Amodeo, A., Balin, I., et al., 2004. Aerosol lidar intercomparison in the framework of EARLINET project: 1. Instruments. Applied Optics 43, 961–976.
Mattis, I., Ansmann, A., Müller, D., Wandinger, U., Althausen, D., 2004. Multiyear aerosol observations with dual-wavelength Raman lidar in the framework of EARLINET. Journal of Geophysical Research 109, D13203. doi:10.1029/2004JD004600.
Mayer, B., Kylling, A., 2005. Technical note: the libRadtran software package for radiative transfer calculations — description and examples of use. Atmospheric Chemistry and Physics 5 (7), 1855–1877.
Menut, L., Flamant, C., Pelon, J., Flamant, P., 1999. Urban boundary layer height determination from lidar measurements over the Paris area. Applied Optics 38, 945–954.
Miller, R.L., Tegen, I., 1998. Climate response to soil dust aerosols. Journal of Climate 11, 3247–3267.
Mok, T.M., Rudowicz, C.Z., 2004. A lidar study of the atmospheric entrainment zone and mixed layer over Hong Kong. Atmospheric Research 69, 147–163.
Müller, D., Mattis, I., Wandinger, U., Ansmann, A., Althausen, D., Stohl, A., 2005. Raman lidar observations of aged Siberian and Canadian forest fire smoke in the free troposphere over Germany in 2003: microphysical particle characterization. Journal of Geophysical Research 110, D17201. doi:10.1029/2004JD005756.
Müller, D., Ansmann, A., Mattis, I., Tesche, M., Wandinger, U., Althausen, D., Pisani, G., 2007. Aerosol-type-dependent lidar ratios observed with Raman lidar. Journal of Geophysical Research 112, D16202. doi:10.1029/2006JD008292.
Myhre, G., Stordal, F., 2001. Global sensitivity experiments of the radiative forcing due to mineral aerosols. Journal of Geophysical Research 106 (D16), 18193–18204.
Noh, Y., Kim, Y., Choi, B., Murayama, T., 2007. Aerosol lidar ratio characteristics measured by a multi-wavelength Raman lidar system at Anmyeon Island, Korea. Atmospheric Research 86, 76–87.
Pappalardo, G., Amodeo, A., Pandolfi, M., Wandinger, U., Ansmann, A., Bösenberg, J., Matthias, V., Amiridis, V., De Tomasl, F., Frioud, M., Iarlori, M., Komguem, L., Papayannis, A., Rocadenbosch, F., Wang, X., 2004. Aerosol lidar intercomparison in the framework of the EARLINET project. 3. Raman lidar algorithm for aerosol extinction, backscatter, and lidar ratio. Applied Optics 43, 5370–5385.
Patterson, E.M., McMahon, C.K., 1984. Absorption characteristics of forest fine particulate matter. Atmospheric Environment 18, 2541–2551.

Perlwitz, J., Tegen, I., Miller, R.L., 2001. Interactive soil dust aerosol model in the GISS GCM 1. Sensitivity of the soil dust cycle to radiative properties of soil dust aerosols. Journal of Geophysical Research 106 (D16), 18167–18192.

Reid, J.S., Hobbs, P.V., Ferek, R.J., Blake, R.J., Martins, J.V., Dunlap, M.R., Liousse, C., 1998. Physical, chemical, and optical properties of regional hazes dominated by smoke in Brazil. Journal of Geophysical Research 103, 32059–32080.

Reid, J.S., Koppmann, R., Eck, T.F., Eleuterio, D.P., 2005. A review of biomass burning emissions part II: intensive physical properties of biomass burning particles. Atmospheric Chemistry and Physics 5, 799–825.

Sanchez, A., Smith, T.F., Krajewski, W.F., 1994. A three-dimensional atmospheric radiative transfer model based on the discrete-ordinates method. Atmospheric Research 33, 283–308.

Turco, R.P., Yu, F., 1997. Aerosol invariance in expanding coagulation plumes. Geophysical Research Letters 24, 1223–1226.

Van Hoosier, M.E., 1996. The Atlas-3 solar spectrum. Available via anonymous ftp at ftp://susim.nrl.navy.mil.

Wandinger, U., Ansmann, A., 2002. Experimental determination of the lidar overlap profile with Raman lidar. Applied Optics 41, 511–514.

Wotawa, G., Novelli, P.C., Trainer, M., Granier, C., 2001. Inter-annual variability of summertime CO concentrations in the Northern Hemisphere explained by boreal forest fires in North America and Russia. Geophysical Research Letters 28, 4575–4578.

Zerefos, C., Ganev, S., Kourtidis, K., Tzortziou, M., Vasaras, A., Syrakov, E., 2000. On the origin of SO2 above Northern Greece. Geophysical Research Letters 27, 365–368.